

Validation of electric transportation system simulation models using multiple performance indexes based on scale and slope evaluation

Jacopo Bongiorno, Andrea Mariscotti, Nicola Pasquino

Abstract—Validation of a simulation model is among other things the evaluation of accuracy against experimental data; quantitative judgment is based on performance indexes that measure various kinds of distances between simulation and data vectors: amplitude, slope, peaks, etc. Different indexes may privilege different characteristics always giving a somewhat biased judgment. For this reason three performance indexes that proved to be effective, robust and reliable are used on a complete test case, which allows verifying which system characteristics may have the most significant impact on validation results. The used performance indexes are Theil, Modified Pendry and FSV (the latter reported in the IEEE Std. 1597.2). The overall judgment of the simulator is “very good”, ranging between good” and “excellent” for various positions and configurations, with the three indexes in substantial agreement, and some minor differences.

Keywords—Electric networks, Modeling, Simulation, Uncertainty, Validation.

I. INTRODUCTION

NUMERIC models are being used more and more often for the assessment of system performance, reliability, safety in normal and exceptional conditions and configurations for a wide range of systems. Correspondingly, simulation model shall undergo a verification and validation process, evaluating its performance for the field of application [1][2]. Depending on it, model suitability may be expressed in terms of accuracy, robustness, reliability [3][4]. The V&V process for a simulation tool is grounded on the initial definition of the intended use, in terms of modeled network elements and necessary information, solution methods for frequency and/or time domain simulation, inclusion of non-linear elements and type of non-linearity, output quantities.

The use of simulation tools aims at replacing experimental methods and measurement campaigns with significant savings in terms of time and cost. There are electrical interoperability phenomena for which the characterization by simulation was already accepted and that appear in standards [4]-[6].

J. Bongiorno is with the University of Genova, Genova, Italy (+39-010-3532169; fax: +39-010-3532700; jacopo.bongiorno@edu.unige.it).

A. Mariscotti is with ASTM Sagl, Chiasso, Switzerland (+41-77-9587584; andrea.mariscotti@astm-e.ch).

N. Pasquino is with the University of Napoli, Napoli, Italy (+39-081-676799; nicola.pasquino@unina.it).

Examples are [7]-[10]:

- the useful voltage, i.e. the average pantograph voltage available when absorbing traction power, calculated per train or per network area;
- the power factor and displacement factor for ac systems, with the same meaning used in industrial supply networks;
- harmonics and inter-harmonics, caused by the interaction of distorting loads and generators, namely trains during power absorption, and the same trains during braking and electric substations;
- dynamic interaction between trains and the supply network, with possible electrical instability, resonances, supply distortion and considerable reactive power flow.

When it is required to evaluate safety-related electrical phenomena, the assessment is the outcome of a very complex, expensive and time consuming process. The use of simulation tools may come into play at two different levels: analysis of a specific case with exhaustive evaluation by means of parametric and sensitivity analysis, maybe supported by experimental confirmation for a few cases; support to the definition of assessment procedures, interference limits and safety margins when defining a standard or procedure.

Despite the electrical equations of each sub-circuit and model cell are in principle simple (component and Kirchhoff equations and basic circuit theory), the interaction of the many network elements and parameters is very complex and results in overall non-linear relationships, that are hardly treated in closed form or with analytical methods.

The verification of a model is the evaluation of the correspondence to the requirements, even for single modules during their development. The validation of a simulation model aims at verifying that it meets its intended use, in terms of overall requirements and user's expectations. The verification phase reviews intermediate elements, by means of static analysis techniques (inspections and reviews) and possibly dynamic techniques (execution of test runs of the simulator modules, maybe assisted by synthetic data). The whole validation process begins with the determination of the model type, its basic attributes and the relations with the system to be modeled [3]. Then, when the model is being formulated and implemented, the model is validated by itself

considering the expected model behavior. But the most relevant part of the validation process is represented by the characterization of the accuracy of model output with respect to the reference data. The validation of a simulator using dynamic techniques is performed by executing test runs on reference cases.

The measurement data and simulator outputs mentioned so far are the electrical quantities of the system (namely voltage, current, impedance), considered as frequency-domain spectra [7]-[9]. They are normally characterized as amplitude and phase response, but real and imaginary part representation lends itself better for pre-processing and data smoothing, avoiding weird behavior at phase reversal (phase wrapping creates discontinuity at $-\pi$ and $+\pi$ transitions).

When comparing simulated and experimental data of this kind, several features normally catch the observer's eye and may be used to quantify the degree of similarity [11][12][13]. The shape of the curves and the relevant distinctive elements (e.g. frequency and amplitude of resonance peaks and anti-peaks, slopes, etc.) orient the choice towards specific performance indexes [13], preferable for several reasons: robustness to noise, adequate response for peaks and slopes, ability to cope with a relatively large uncertainty of experimental data.

More than one performance index is used for the validation, in order to cross-check the indexes themselves and avoid biasing and distortion of validation results. Comparing performance index values is of course not so straightforward, because they have different ranges and different sensitivities to curve characteristics: they were tested extensively on sample curves in [12].

In this work, first, the Theil and the Modified Pendry indexes are selected because they showed to be consistent and stable and they are compatible and may be evaluated against a linear scale between 0 and 1 [13]; afterwards indexes based on the FSV validation technique are used to perform a more complete analysis. These indexes are applied to the simulation output comparing it to reference experimental data that for our purpose are assumed accurate and characterized by a negligible uncertainty. The test case and the experimental data refer to the Velim test ring, which is a short railway line where rolling stock is normally tested for homologation; details of the nature of acquired data and the type of performed tests are given in Section 2. The cited validation indexes are recalled at the beginning of Section 3, where the results of comparisons between simulation results and experimental data are reported.

II. PERFORMANCE INDEXES AND REFERENCE DATA

As said in the Introduction, the focus of this work is on the indexes used to evaluate model adequacy and the degree of similarity between simulation and experimental data, where "similarity" indicates a quantitative evaluation of the distance between the two vectors \mathbf{o} (simulation output) and \mathbf{m} (measured data). Different types of distances may be applied as they appear in the performance indexes that are reviewed

and evaluated in the following: absolute deviation, maximum absolute deviation, root mean square, amplitude and slope difference, etc. The concepts of distance and correlation may be used to establish similarity between vectors. However, from a general viewpoint, when evaluating the correctness and adequacy of a simulation model, the judgment is based on the visualization of many output results. Inspecting visually the results and basing the judgment upon this has its strong and weak sides:

- the eye concentrates on peak positions and slopes, ignoring exact values; visual evaluation selects the most relevant behavior and trend, rejecting many details with adverse influence;
- the amount and organization of data may be too large and complex to be compared visually with ease and in this case selection and feature extraction shall be implemented.

A. Theil inconsistency coefficient [14]

The Theil inconsistency coefficient U is expressed in the following form:

$$U = \frac{\sqrt{\sum_{j=0}^{N-1} (o_j - m_j)^2}}{\sqrt{\left[\sqrt{\sum_{j=0}^{N-1} o_j^2} + \sqrt{\sum_{j=0}^{N-1} m_j^2} \right]}} \quad (1)$$

U is limited between 0 and 1: the lower its value, the more consistent the two data vectors.

It is a classical root mean square error, normalized by the rms values of the \mathbf{o} and \mathbf{m} data vectors; it is very similar to the concept of normalized covariance of two distributions. The Theil index is an amplitude-only index: by inspection of (1) it may be said that it has no singular points, but it is affected by mean value data, it is hence used together with a very simple normalization that make the mean value equal to 0.

B. Pendry correlation factor [15]

Pendry correlation factor is used instead when the two sequences have many variations (i.e. "peak and valleys"). The objective in [15] was to locate small peaks around large peaks, where the former could be masked by background noise; when transferred to electric networks this situation occurs when estimating highly damped non-dominant poles in the presence of strong resonances. By taking the fractional (or logarithmic) first derivative $L = x'/x$ of either the model output o or the experimental data m , an expression Y is built around it

$$Y = \frac{L^{-1}}{(L^{-2} + K^2)} \quad (2)$$

where K is a constant derived from the physical nature of the phenomenon and in general might be adjusted to trim the range of variation of L .

The Pendry reliability index is thus defined in our case by distinguishing the Y calculated on model output Y_o and the one calculated on experimental results Y_m . The original formulation

is quadratic and it is not limited to unity; for this reason in [12][13] it was proposed a modified expression using linear quantities, R_{PL} , that limits the maximum variation of the index to 1:

$$R_{PL} = \frac{\sum_{i=0}^{N-1} |L_{oi} - L_{mi}|}{\sum_{i=0}^{N-1} (|L_{oi}| + |L_{mi}|)} \quad (3)$$

Using R_{PL} , saturation to unity for extremely different curves is assured.

C. Feature Selective Validation [16]

Feature Selective Validation (FSV) technique is a method to determine the level of agreement between two or more data sets, accepted and described in IEEE Std. 1597.2 [16]. The purpose of the method is to quantify changes and variations, and give an overall evaluation about the similarity of the analyzed data.

The validation by means of FSV method is more complex and elaborated than with Theil or Pendry indexes. Data sets, after being brought to the same number of points, are Fourier transformed and separated into three parts: dc, lo and hi vectors. These three sub-vectors correspond to: the dc portion (corresponding to the first four data points), the low and the high frequency portions, the latter separated by a break point index I_b set at the 40% of the data set intensity.

$$S = \sum_{i=5}^{N-1} X(i) \quad I_b : \sum_{i=5}^{I_b} X(i) = 40\% S \quad (4)$$

where $X(i)$ indicate the transformed data $x(i)$.

These sub-vectors are zero padded to the original length of the entire data set vector and anti-transformed obtaining the vectors that are used for the validation and calculation of FSV indexes: dc, lo and hi. The FSV indexes are: Amplitude Difference Measure (ADM) to evaluate the amplitude differences, Feature difference Measure (FDM) to evaluate the differences between the features of the data sets and Global Difference Measure (GDM) to evaluate the overall difference. All indexes are vectors with the same initial length; they are displayed and evaluated by means of histogram and “Grade and Spread” values.

Here below from eq. (5) to (14) the formulation of the FSV indexes is reported for completeness, where o and m are the input data sets, and the subscripts “dc”, “lo” and “hi” indicate the three sub-vectors determined as explained above.

$$ADM_i = \left| \frac{|o_{lo,i}| - |m_{lo,i}|}{\frac{1}{N} \sum_{j=0}^{N-1} |o'_{lo,j}| + |m'_{lo,j}|} \right| + |ODM_i| \exp^{ODM_i} \quad (5)$$

$$ODM_i = \frac{x_i}{\delta_i} = \frac{|o_{dc,i}| - |m_{dc,i}|}{\frac{1}{N} \sum_{i=0}^{N-1} |o_{dc,i}| + |m_{dc,i}|} \quad (6)$$

$$ADM = \sum_{i=0}^{N-1} ADM_i \quad (7)$$

$$FDM_i^1 = \frac{|o'_{lo,i}| - |m'_{lo,i}|}{\frac{2}{N} \sum_{j=0}^{N-1} |o'_{lo,j}| + |m'_{lo,j}|} \quad (8)$$

$$FDM_i^2 = \frac{|o'_{hi,i}| - |m'_{hi,i}|}{\frac{6}{N} \sum_{j=0}^{N-1} |o'_{hi,j}| + |m'_{hi,j}|} \quad (9)$$

$$FDM_i^3 = \frac{|o''_{hi,i}| - |m''_{hi,i}|}{\frac{7.2}{N} \sum_{j=0}^{N-1} |o''_{hi,j}| + |m''_{hi,j}|} \quad (10)$$

$$FDM_i = 2|FDM_i^1 + FDM_i^2 + FDM_i^3| \quad (11)$$

$$FDM = \sum_{i=0}^{N-1} FDM_i \quad (12)$$

$$GDM_i = \sqrt{(ADM_i)^2 + (FDM_i)^2} \quad (13)$$

$$GDM = \sum_{i=0}^{N-1} GDM_i \quad (14)$$

D. Evaluation of index values

The three performance indexes are evaluated for each test case used in the validation process, extracting a general judgment that goes beyond the numeric value. To this aim, similarly to the FSV index recommended in the IEEE Std. 1597.2 [16], six sub-intervals are selected: Excellent (Ex), Very Good (VG), Good (Go), Fair (Fa), Poor (Po) and Very Poor (VP). The result is shown in Table I.

TABLE I. INTERPRETATION SCALE FOR THEIL, MOD. PENDRY AND FSV INDEXES

Lower bound	Upper bound	Quality descriptor
0.0	0.1	Excellent
0.1	0.3	Very Good
0.3	0.5	Good
0.5	0.7	Fair
0.7	0.9	Poor
0.9	1.0	Very Poor

The FSV output are histograms that show the normalized number of points of the ADM_i , FDM_i and GDM_i indexes which fall in each bin and are labeled thus by a quality descriptor, supported by the Spread and Grade which represent the

dispersion and the skewness of the histograms. The Spread value indicates the number of classes that contain the 85% of the values beginning from the highest bar. Grade value, instead, indicates the number of the interval in the interpretation scale whose cumulative distribution contain the 85% of the values beginning from the Excellent class. High values of Spread indicate that the histogram is much dispersed and hence that the result attributed to the highest bar in the histogram has an unsatisfactory level of confidence; on the other hand a Spread value ≤ 1 indicates a very high level of confidence. The Grade quantifies the distribution of the Histogram bars: low values indicate that the majority of the index data fall in the first part of the histogram, which indicates a good comparison; high values, instead, indicate a large dispersion of the histogram values or that the majority of the index data fall in the second part of histogram, ranking the comparison as poor.

E. Data vectors

The electrical quantities of the system considered for the validation are the pantograph voltage V_p and current I_p , manipulated as frequency-domain spectra, extracting the pantograph impedance $Z_p = V_p/I_p$, that is used for the validation. The reason for using Z_p is to have a quantity that i) is independent on the specific voltage or current intensity, provided that measurement problems related to sensitivity and noise are not of concern, ii) behaves in a known pattern that is enough regular to be interpreted, and iii) is considered a relevant quantity for analysis of rolling stock emissions and network stability.

The tested frequencies are between 50 Hz and 20 kHz, using the odd harmonics of the supply frequency (150, 250, 350 ... Hz). The reason is explained below while evaluating the quality of the measurement results.

The frequency analysis is done with a Discrete Fourier Transform using a Hamming smoothing window to reduce the frequency leakage and applying synchronous extraction of the time epoch T_w for the transform by separately estimating the instantaneous frequency (only approximately 50 Hz [17][18]). The procedure is the same as described in [19]: i) a first spectrum is computed using a coarse estimate of the supply frequency f'_1 ; ii) interpolation of the frequency bins gives a more accurate estimate of the instantaneous fundamental frequency f''_1 , suitable for our purpose; iii) the spectrum is then recalculated.

The frequency resolution is 10 Hz ($T_w=100$ ms) and $P=10$ successive epochs with 50% overlap (for a total of $Q=2P-1=19$ epochs) are used to extract the average spectrum, that is then used to extract the relevant frequency points at odd multiples of 50 Hz for the successive analysis. The total time length of the collected epochs for one spectrum is $T_i = P T_w = 1$ s. Spectra are then smoothed with a median filter to remove small artifacts due to local variability of a few voltage or current spectral components and noise.

III. VALIDATION ON THE VELIM CASE STUDY

The simulation models and parameters were initially validated based on sample measurements taken along the Italian network [11] and at the Velim test ring in controlled conditions of low voltage feeding and short and open circuit at the far end [13]: the fitting of simulated and experimental curves was in general good and allowed to test several indexes of performance. The Italian network was modeled using average values for various elements (such as cable connections, supply transformers, etc.), because of lack of specific information for the tested network section. Average or nominal values are normally known by datasheets and test bulletins, past measurement campaigns and common knowledge; however, several electrical parameters that are quite relevant to model behavior and simulation results (e.g. stray parameters) are not well covered by standard testing and may be thus in general much more variable from unit to unit than other quantities and characteristics, that are subject to requirements and testing. The validation suffers thus a general uncertainty due to the incomplete description of the reference system.

A further test campaign was performed to collect data to be used for confirmation of the models and theory developed in the European Project EUREMCO [20]. Test runs were performed at the Velim test centre in Czech Republic in 2014 [21].

A. Velim test ring

The Velim test ring is well maintained and the personnel know possible critical deviations from nominal (or normal) values, because tests are done routinely every week (in many cases every day). Additionally, the test circuit was studied extensively for some days, thanks to the received support and also to its limited extension.

The test centre features two single track test rings: the smaller one has a length of 6 km and is surrounded by the bigger one that is about 13.2 km long. The inner ring is not included in the model because during the measurements it was sectioned.

The big test ring has a cross section featuring six conductors along its length. Rails are connected together (transversal bonding) every 300 m, except in the track circuit testing area between chainage km 10.672 and 11.672; the two catenary (positive) feeders are connected with the contact line and messenger every 120 m.

The test ring was connected to the 25 kV 50 Hz power supply substation (single-phase transformer, fed by the High Voltage national grid) and a train consist (two wagons trailed by a BB36000 loco manufactured by Alstom) travelled along the ring performing accelerations and braking in the two straight parts of the track. Positions are thus four in the first line section A and four in the second line section B, identified by their chainage as: A1=km 8.3, A2=km 8.0, A3=km 7.4 and A4=km 7.1; B1=km 1.6, B2=km 1.3, B3=km 1.0 and B4=km 0.4.

These results are used here to validate the simulation model in real conditions of use, including the 110 kV/25 kV single-phase supply transformer, the feeding cables and the loco input transformer circuit. The scheme of the test ring and measurement positions is shown in Fig. 1.

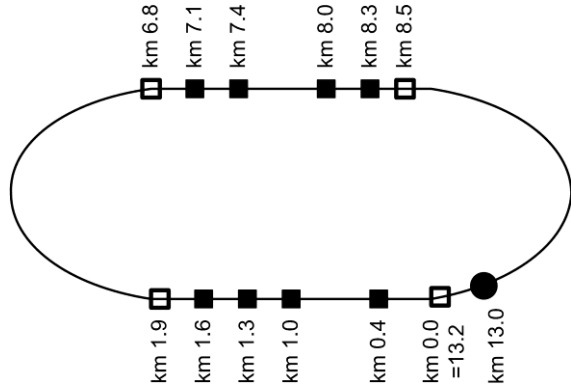


Fig. 1. Scheme of the Velim test ring with supply substation (circle), test positions (filled squares) and other reference positions (hollow squares)

The line model, as done for other study cases [11], includes frequency-dependent inductance and losses of the return circuit elements and stray parameters, in particular rail-to-earth conductance, considering the effect of the interconnection of the track of the outer ring, that of the inner ring and the cable screens and the negative pole of the transformer secondary.

Additionally, the influence of the HV feeder is difficult to model because only the nominal values are known, and a rough estimate of the 110 kV network indicates the possibility of resonance effects in the same frequency range where the supply transformer has its short-circuit resonance (i.e. around 10 kHz).

B. Evaluation of experimental data

Experimental data are characterized by a variable uncertainty depending on the train operating conditions and on the portions of the frequency intervals: low current amplitude gives more noisy spectra and a larger uncertainty, so in braking and cruising conditions, and at resonances (where the maxima of pantograph impedance are located); moreover, at low frequency the variability of the characteristic harmonics of the locomotive (and on-board traction converters) causes a remarkable increase of data dispersion, so that these samples were heavily post-processed and smoothed to recover a better shape and in the end have been discarded (validation uses data samples at frequencies above 1.6 kHz).

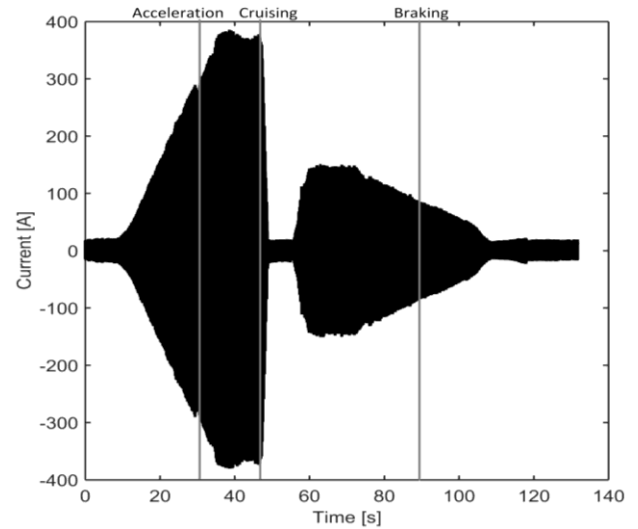


Fig. 2. Pantograph current waveform with three different locomotive operating conditions during a test run: Acceleration, Cruising, Braking.

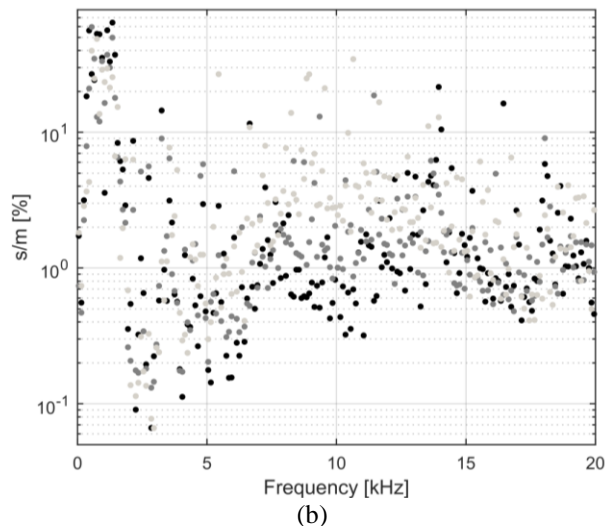
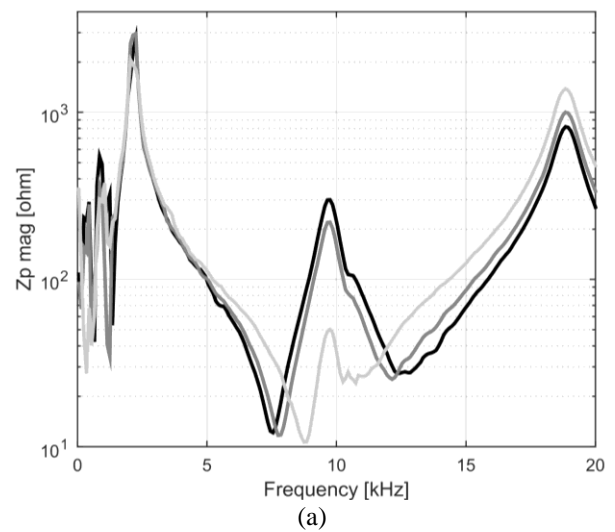


Fig. 3. (a) Magnitude of pantograph impedance and (b) normalized standard deviation s/m, for accel. (black), cruising (gray), brak. (light gray).

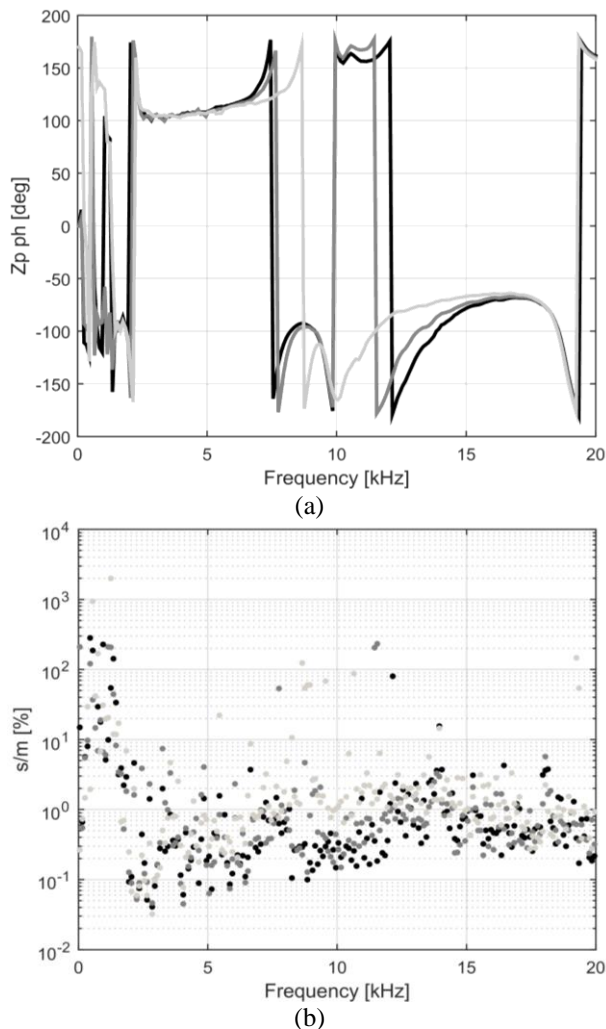


Fig. 4. (a) Phase of pantograph impedance and (b) normalized standard deviation s/m , for accel. (black), cruising (gray), brak. (light gray).

The pantograph impedance Z_p is calculated in magnitude and phase for the eight positions A1-A4 and B1-B4 along the test ring. Since at each position the train is in either acceleration, cruising or braking condition, the three behaviors, identified in the current waveform of Fig. 2, are exemplified in Fig. 3 and Fig. 4 together with an estimate of sample dispersion s , normalized to the mean value m . Discarding data samples below 1600 Hz ensures that the relative dispersion is always better than 10%, on average around 3%, excluding a few data points around resonances; this may be translated at a first approximation in the order of magnitude of the uncertainty of performance index output.

It is evident, observing the behavior of pantograph impedance curves in Fig. 3(a), that there is a relationship with the different locomotive position along the test ring, in particular for the portion of the curve near the anti-resonance, as well as for the amplitude of the second resonance at 10 kHz. Graphs in the part (b) of the Fig. 3 and Fig. 4 indicate an increased dispersion of data when the current in the system is low; for higher current level there is no relevant difference between acceleration and cruising conditions.

C. Visual comparison results

A first validation of the magnitude and phase curves is done by visually comparing simulated and measured data. The curves for section A and B are shown in Fig. 5 and Fig. 6 for some of the various locomotive positions. In Section A discrepancies are evident for magnitude at the main and second resonance; it is remembered that the latter occurring at 10kHz is caused by the interaction of the transformer with the High Voltage supply grid, which couldn't be modeled accurately. For section B, at some distance and thus decoupled from the substation transformer, the agreement between simulation and measurement curves relevant, both in magnitude and in phase.

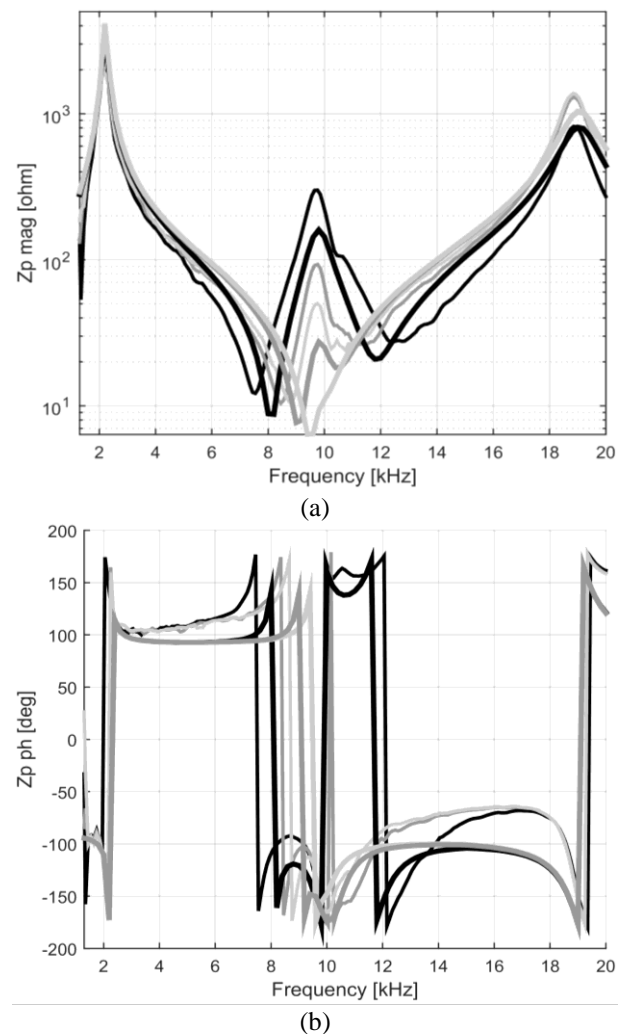


Fig. 5. Pantograph impedance comparison (a) magnitude and (b) phase, in test section A (km 8.3, 8, 7.1 from darkest to lighter line), measured (thin lines) and simulated (thick lines).

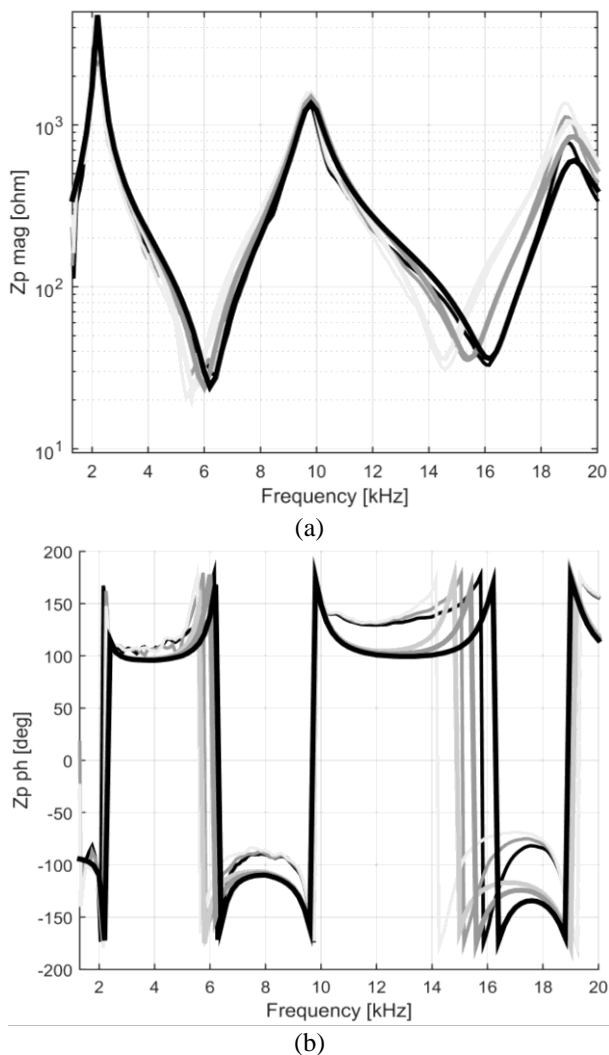


Fig. 6. Pantograph impedance comparison (a) magnitude and (b) phase, in test section B (km 1.6, 1.0, 0.1, from darkest to lighter line), measured (thin lines) and simulated (thick lines).

The visual comparison is useful to indicate the global impression about the similarity of the curves; however it is based only on the evaluator's experience and cannot give quantitative indications of the similarity with experimental data. This is addressed in the following sections using performance indexes for a more objective comparison.

D. Theil and Mod. Pendry results

The results of the calculation of indexes values are reported in Table II and Table III for the two considered sections (A and B). According to the interpretation scale reported in sec. II.D, the associated qualitative values are also shown. It is underlined that both indexes give an overall evaluation, but no indication about where the most relevant differences are located and if they are due to differences in amplitude, slope or shape.

TABLE II. THEIL AND MOD. PENDRY INDEXES FOR THE MAGNITUDE AND PHASE OF Z_p CURVES IN RING SECTION A

Magnitude	km 8.3	km 8.0	km 7.4	km 7.1
Theil	0.186 (VG)	0.152 (VG)	0.259 (VG)	0.269 (VG)
Mod. Pendry	0.279 (VG)	0.275 (VG)	0.305 (G)	0.330 (G)
Phase	km 8.3	km 8.0	km 7.4	km 7.1
Theil	0.201 (VG)	0.195 (VG)	0.178 (VG)	0.169 (VG)
Mod. Pendry	0.135 (VG)	0.100 (Ex)	0.046 (Ex)	0.054 (Ex)

Results in Table II indicate that the similarity for magnitude and phase has opposite behavior, the former getting worse for train position towards km 7.1. For ring section B the similarity is in general better, but the Theil and Modified Pendry indexes do not fully agree on which train position gives the worst results; the differences between positions are such that position at km 1.6 may be identified as the best one, but all others follow with a difference around 20% on average: Theil index identifies curves at km 1.3 as the worst ones, while Mod. Pendry those at km 0.4.

TABLE III. THEIL AND MOD. PENDRY INDEXES FOR THE MAGNITUDE AND PHASE OF Z_p CURVES IN RING SECTION B

Magnitude	km 1.6	km 1.3	km 1.0	km 0.4
Theil	0.135 (VG)	0.280 (VG)	0.245 (VG)	0.249 (VG)
Mod. Pendry	0.174 (VG)	0.199 (VG)	0.190 (VG)	0.207 (VG)
Phase	km 1.6	km 1.3	km 1.0	km 0.4
Theil	0.139 (VG)	0.133 (VG)	0.121 (VG)	0.125 (VG)
Mod. Pendry	0.091 (Ex)	0.042 (Ex)	0.036 (Ex)	0.067 (Ex)

Considering globally the comparison, both Theil and Modified Pendry indexes are in agreement, indicating a good or very good similarity between curves and, in some cases, for phase values an excellent similarity.

E. FSV results

The validation of pantograph impedance curves is thereafter performed by means of the FSV technique. Amplitude and phase curves are considered and results are reported for all the FSV indexes, as statistic quantities, histograms and point by point index values. The interpretation of the histograms is supported by the evaluation of the mean value, Grade and Spread of the index. Mean values can be evaluated using the criteria exposed in Table I, while Grade and Spread, comprised in the 0-6 interval, give indications about the confidence of the results. A narrower Spread implies a higher confidence, while Grade gives indication about the portion of histogram where 85% of elements lie [16]. The point by point visualization of the two FSV indexes ADM and FDM gives

also information about the weakest portions of the curves, for both amplitude and shape similarity.

Two sample curves are shown, that by the way are quite representative of all curves for sections A and B (see Fig. 7 and Fig. 8).

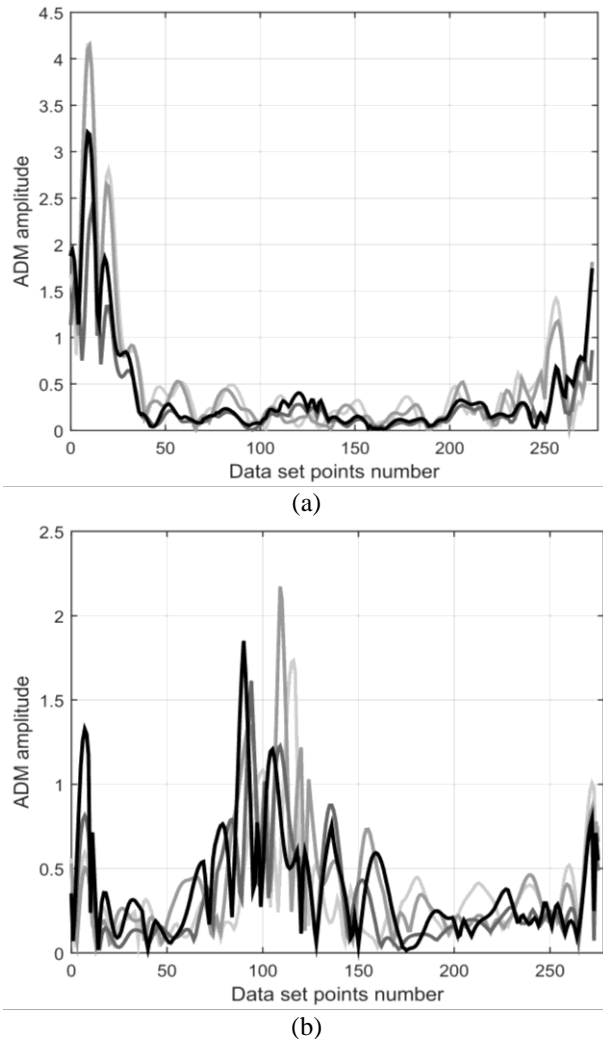


Fig. 7. Amplitude of ADM from pantograph impedance comparison (a) magnitude and (b) phase, in test section A at km 8.3, 8. 7.4. 7.1, (from dark gray to light gray).

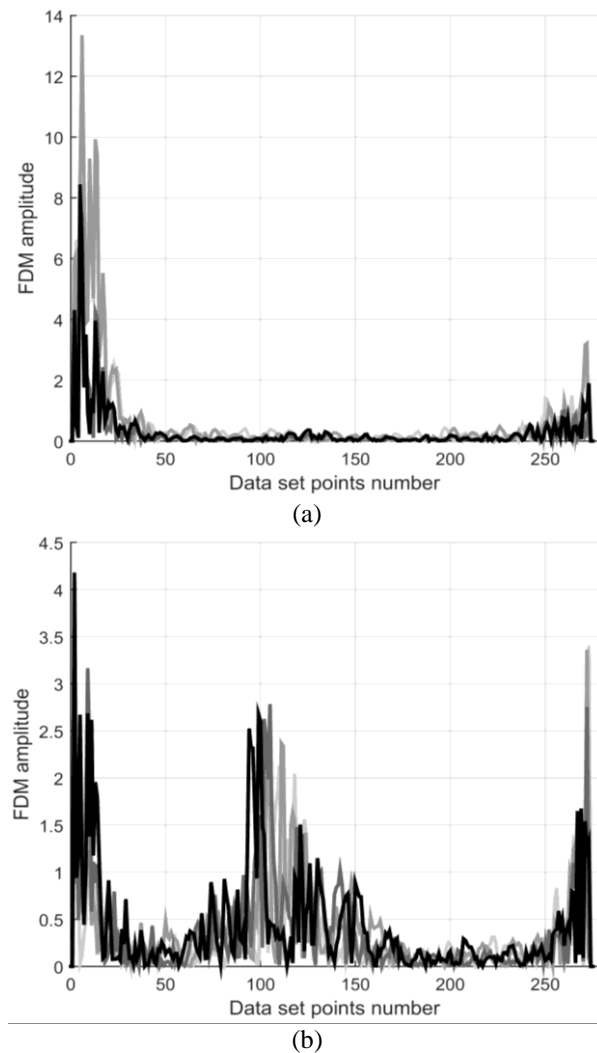


Fig. 8. Amplitude of FDM from pantograph impedance comparison (a) magnitude and (b) phase, in test section A at km 8.3, 8. 7.4. 7.1, (from dark gray to light gray).

The ADM differences for the magnitude are in the first and last part of the curves, whereas for the phase curves the differences are located in the central part. This underlines the fact that the resonance at 10 kHz due to the HV grid is not fully matched, while — even if with some minor deviation — the other two resonances are well modeled.

The FDM index points at the mismatch in the slope of the curves occurring again around the 10 kHz resonance, although the 10 kHz resonance frequency is correctly identified in the model. Moving towards the substation the error around 10 kHz increases, as indicated by the light gray curves.

Last, the oscillations that are visible in the curves are due to the leakage caused by the double transform operation to obtain dc, lo and hi vectors.

The ADM histograms are shown in Fig. 9 and Fig. 10, for each section A and B of the test circuit. The interpretation of the histograms is supported by the evaluation of the mean value, Grade and Spread of the index reported in Table IV and Table V for section A and B, respectively.

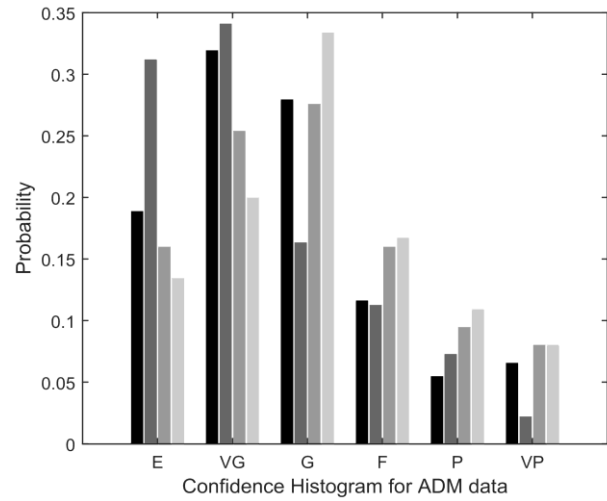
TABLE IV. ADM VALUES MAGNITUDE AND PHASE OF Z_p CURVES IN RING SECTION A

Magnitude	km 8.3	km 8.0	km 7.4	km 7.1
Mean ADM	0.391	0.291	0.496	0.548
Spread ADM	4	4	5	5
Grade ADM	4	4	5	5
Phase	km 8.3	km 8.0	km 7.4	km 7.1
Mean ADM	0.373	0.320	0.392	0.329
Spread ADM	4	4	4	4
Grade ADM	4	4	4	4

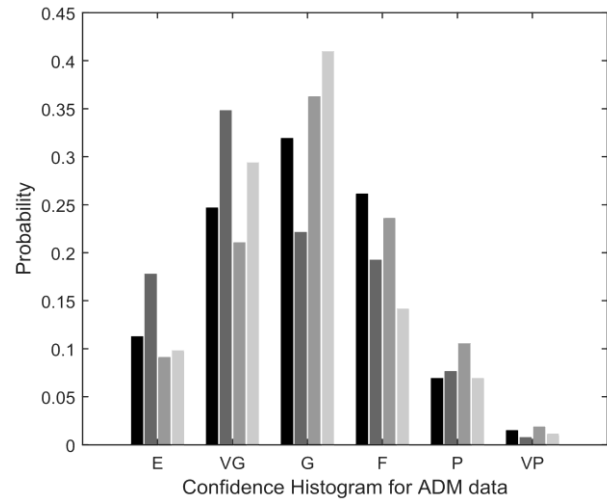
The amplitude differences between the magnitudes of pantograph impedance curves for test section A are larger moving towards the substation, when the interaction of the national supply grid becomes more influent, creating a resonance peak at about 10 kHz (lacking accurate data of High Voltage grid modeling was only approximate). The results of the validation are anyway good, as well as the confidence level, except for locomotive at km 7.4 and 7.1 where the mean ADM leads to a Fair similarity between curves. ADM results considering the phases of pantograph impedance are, as expected, uniformly indicating Good similarity and good confidence.

TABLE V. ADM VALUES MAGNITUDE AND PHASE OF Z_p CURVES IN RING SECTION B

Magnitude	km 1.6	km 1.3	km 1.0	km 0.4
Mean ADM	0.212	0.416	0.354	0.390
Spread ADM	3	4	4	4
Grade ADM	3	4	4	4
Phase	km 1.6	km 1.3	km 1.0	km 0.4
Mean ADM	0.241	0.279	0.231	0.263
Spread ADM	3	3	3	3
Grade ADM	3	4	3	4



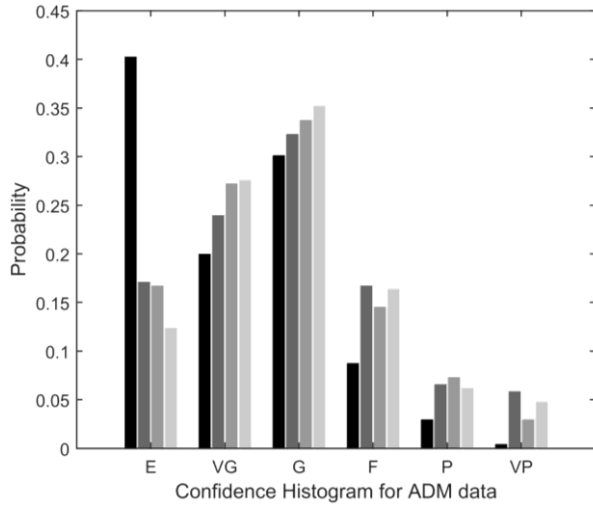
(a)



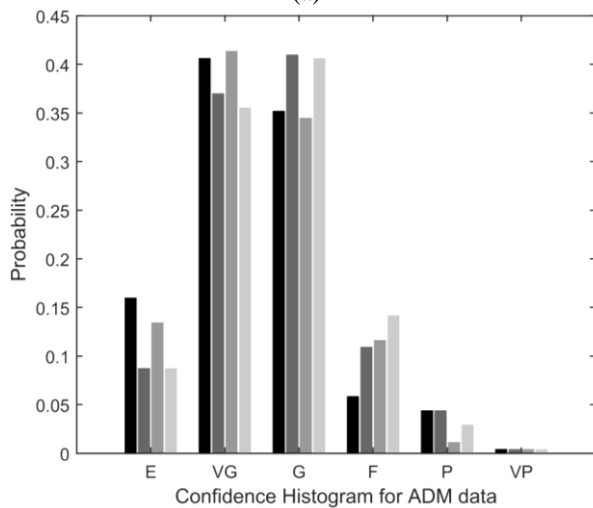
(b)

Fig. 9. Confidence Histogram of ADM, from pantograph impedance comparison, (a) magnitude and (b) phase, for data at km 8.3, 8. 7.4. 7.1 (from dark to light gray bar).

The validation results for test section B show a more uniform behavior; Grade and Spread values indicate good confidence of the validation results. A significant result is achieved at km 1.6, where the histogram bar indicates an “excellent” score (see Fig. 10(a)).



(a)



(b)

Fig. 10. Confidence Histogram of ADM, from pantograph impedance comparison, (a) magnitude and (b) phase, for data at km 1.6, 1.3, 1, 0.4 (from dark to light gray bar).

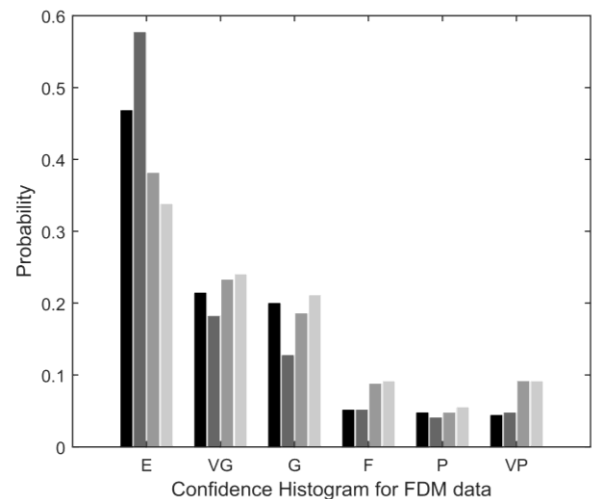
The FDM results are shown in Fig. 11 and Fig. 12. As for ADM, the least similar curves are for the two positions closest to the substation, as far as the Z_p magnitude is concerned. For the phase the agreement is better and the worst position is at km 8.3 of section A. In any case all the comparisons are scored as Excellent or Very Good.

TABLE VI. FDM VALUES MAGNITUDE AND PHASE OF Z_p CURVES IN RING SECTION A

Magnitude	km 8.3	km 8.0	km 7.4	km 7.1
Mean FDM	0.322	0.297	0.651	0.694
Spread FDM	3	3	4	4
Grade FDM	3	3	4	4
Phase	km 8.3	km 8.0	km 7.4	km 7.1
Mean FDM	0.415	0.380	0.392	0.356
Spread FDM	5	5	4	4
Grade FDM	5	5	4	4

TABLE VII. FDM VALUES MAGNITUDE AND PHASE OF Z_p CURVES IN RING SECTION B

Magnitude	km 1.6	km 1.3	km 1.0	km 0.4
Mean FDM	0.267	0.618	0.517	0.529
Spread FDM	4	4	4	4
Grade FDM	4	4	4	4
Phase	km 1.6	km 1.3	km 1.0	km 0.4
Mean ADM	0.241	0.279	0.231	0.263
Spread FDM	3	3	3	3
Grade FDM	3	4	3	4



(a)

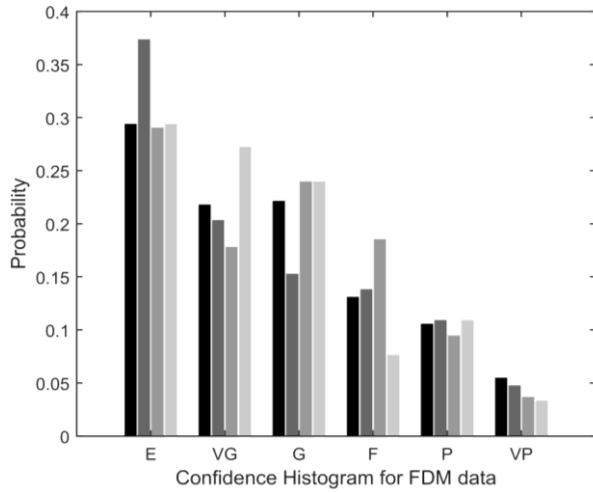
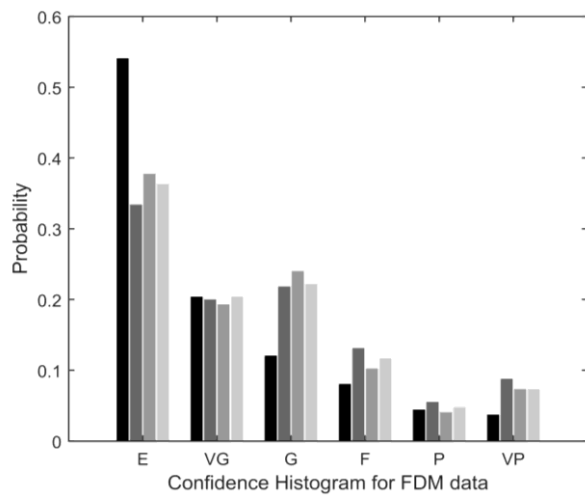
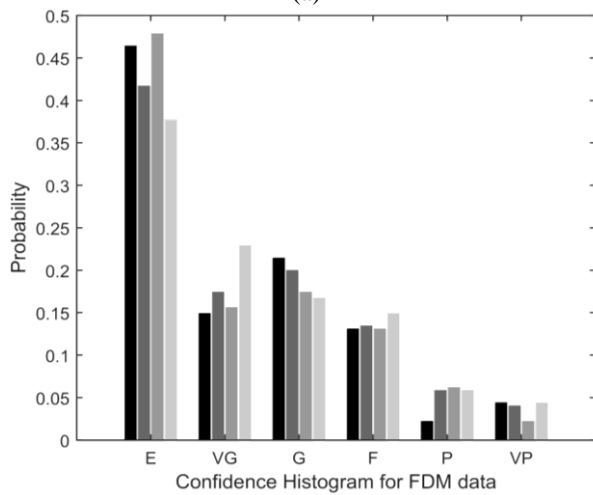


Fig. 11. Confidence Histogram of FDM, from pantograph impedance comparison, (a) magnitude and (b) phase, for data at km 8.3, 8. 7.4. 7.1 (from dark to light gray bar).



(a)



(b)

Fig. 12. Confidence Histogram of FDM, from pantograph impedance comparison, (a) magnitude and (b) phase, for data at km 1.6, 1.3, 1, 0.4 (from dark to light gray bar).

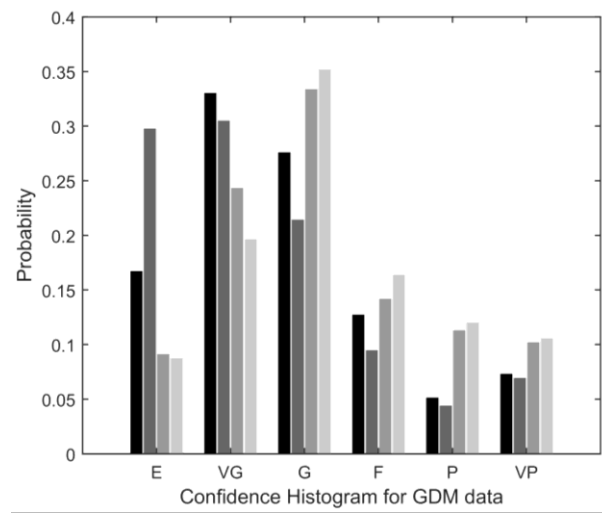
(Fig. 13) and Very Good or Good judgments when the locomotive runs in test section B (Fig. 14).

TABLE VIII. GDM VALUES MAGNITUDE AND PHASE OF Z_p CURVES IN RING SECTION A

Magnitude	km 8.3	km 8.0	km 7.4	km 7.1
Mean GDM	0.478	0.409	0.828	0.894
Spread GDM	4	4	5	5
Grade GDM	4	4	5	5
Phase	km 8.3	km 8.0	km 7.4	km 7.1
Mean GDM	0.557	0.487	0.615	0.541
Spread GDM	4	4	4	4
Grade GDM	5	5	5	5

TABLE IX. GDM VALUES MAGNITUDE AND PHASE OF Z_p CURVES IN RING SECTION B

Magnitude	km 1.6	km 1.3	km 1.0	km 0.4
Mean GDM	0.324	0.809	0.692	0.720
Spread GDM	4	4	4	4
Grade GDM	4	5	4	5
Phase	km 1.6	km 1.3	km 1.0	km 0.4
Mean GDM	0.364	0.415	0.349	0.409
Spread GDM	3	3	3	3
Grade GDM	4	4	4	4



(a)

The GDM indicates results between Good and Fair for comparison of curves with the locomotive in test section A

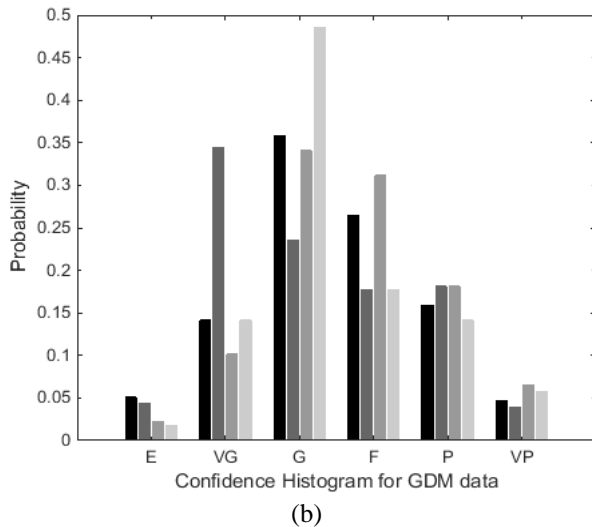


Fig. 13. Confidence Histogram of GDM, from pantograph impedance comparison, (a) magnitude and (b) phase, for data at km 8.3, 8. 7.4, 7.1, (from darkest to lighter bar).

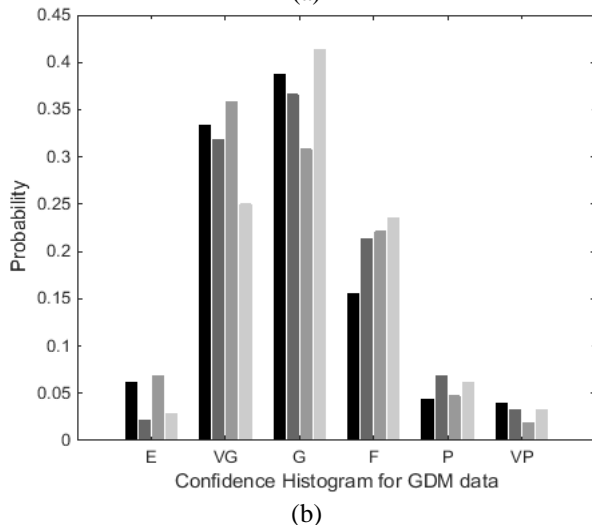
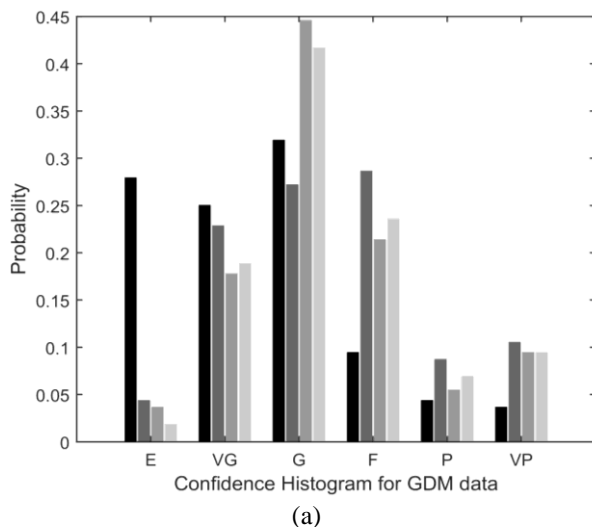


Fig. 14. Confidence Histogram of GDM, from pantograph impedance comparison, (a) magnitude and (b) phase, for data at km 1.6, 1.3, 1, 0.4, (from darkest to lighter bar).

IV. CONCLUSION

The validation of the simulation model of the Velim test ring in real operating conditions was made, using real measurements, performed in well known conditions (regarding network parameters, train operating conditions and absence of other trains); only the High Voltage feeding line before the 25 kV transformer is modeled approximately. An evaluation of the dispersion of measurement data used for the validation was preliminarily performed indicating, as expected, higher dispersion for low current conditions; similarly low frequency bins are influenced by rolling stock characteristic harmonics and have an intolerable dispersion, so that they were discarded and the performance indexes evaluated only above 1.6 kHz.

A preliminary visual comparison of simulated and measured results is done, spotting out a better similarity between curves of test section B than that of test section A.

Two validation indexes reviewed and verified in previous work [12][13] are initially considered for a quantitative assessment: the Theil and the Modified Pendry indexes are applied to the measured and simulated pantograph impedance curves. The indexes give encouraging result, scoring the similarity as Good or Very Good, and in some case Exceptional, allowing to conclude that the model has been positively validated. However, these indexes are not able to identify the weak points of the model or to selectively compare specific characteristics of the curves, such as shape, amplitude, slope, etc. To this aim a more complete and articulated validation tool has been used: the Feature Selective Validation (FSV) tool, an internationally recognized validation method for electromagnetic computation.

FSV indicates a Very Good or Good agreement between simulations and measurement results, confirming the positive validation made by the former indexes. FSV has given also information about the characteristics of the curves, indicating the resonance due to the High Voltage supply network as the main cause of discrepancy.

ACKNOWLEDGMENTS

The authors wish to warmly thank the support of VUZ (Výzkumný Ústav Železniční a.s.) personnel at the Velim Test Centre, Czech Republic, and in particular Mr. Karel Peška and Mr. Aleš Stopka.

REFERENCES

- [1] M.U. Brandolini, C. Briano, E. Briano and R. Revetria, "VV&A of Complex Modeling and Simulation Systems: Methodologies and Case Studies," *International Journal of Mathematics and Computers in Simulation*, Vol. 2, n. 4, 2008, pp. 338-348.
- [2] M. Panoiu and F. Neri, "Open research issues on Modeling, Simulation and Optimization in Electrical Systems," *WSEAS Transactions on Systems*, Vol. 13, 2014, pp. 332-334.
- [3] A. Mariscotti, "On the validation of models of large complex electrical systems," *International Journal of Measurement Technologies and Instrumentation Engineering*, Vol. 5, n. 1, Jan.-March 2015.
- [4] Railway applications – Fixed installations – Requirements for the validation of simulation tools used for the design of traction power supply systems, CENELEC C20 working document, May 2012.

- [5] European Union, Technical Specifications for Interoperability – Energy System, 2002/733, 30-05-2002.
- [6] Railway applications. Power supply and rolling stock. Technical criteria for the coordination between power supply (substation) and rolling stock to achieve interoperability, CENELEC EN 50388 Standard, Aug. 2005.
- [7] A. Mariscotti, "Direct Measurement of Power Quality over Railway Networks with Results of a 16.7 Hz Network," *IEEE Transactions on Instrumentation and Measurement*, Vol. 60, n. 5, May 2011, pp. 1604-1612.
- [8] A. Mariscotti, "Results on the Power Quality of French and Italian 2x25 kV 50 Hz railways", I2MTC 2012, Graz, Austria, May 13-16, 2012.
- [9] A. Mariscotti, "Measuring and Analyzing Power Quality in Electric Traction Systems", *International Journal of Measurement Technologies and Instrumentation Engineering*, Vol. 2 n. 4, Oct.-Dec. 2012, pp. 21-42.
- [10] J. Bongiorno and A. Mariscotti, "Recent Results on the Power Quality of the Italian 2x25 kV 50 Hz Railway", 20th Imeko TC4 International Symposium, Benevento (Italy), Sept. 15-17, 2014.
- [11] J. Bongiorno and A. Mariscotti, "Experimental validation of the electric network model of the Italian 2x25 kV 50 Hz railway," 20th Imeko TC4 International Symposium, Benevento (Italy), Sept. 15-17, 2014.
- [12] J. Bongiorno and A. Mariscotti, "Performance of indexes used for model validation," Proceedings of CSECS 2014, Lisbon, Portugal, Oct. 30 – Nov. 01, 2014.
- [13] J. Bongiorno and A. Mariscotti, "Evaluation of performances of indexes used for validation of simulation models based on real cases," *International Journal of Mathematical Models and Methods in Applied Sciences*, Vol. 9, 2015, pp. 22-43.
- [14] H. Theil, *Economics and Information Theory*, Amsterdam, North-Holland, 1967.
- [15] J.B. Pendry, "Reliability factors for LEED calculations," *Journal of Physics – Part C: Solid State Physics*, Vol. 13, pp. 937-944, 1980.
- [16] IEEE Std. 1597.2, *Recommended Practice for Validation of Computational Electromagnetics Computer Modeling and Simulations*, 2010.
- [17] A. Mariscotti and D. Slepicka, "The Frequency Stability of the 50 Hz French Railway", I2MTC 2012, Graz, Austria, May 13-16, 2012.
- [18] R. Lapuh and A. Mariscotti, "Performance of three algorithms for the fundamental frequency estimation against 16.7 Hz railways data", I2MTC 2012, Graz, Austria, May 13-16, 2012.
- [19] J. Bongiorno, A. Mariscotti, "Variability of pantograph impedance curves in DC traction systems and comparison with experimental results", *Przegląd Elektrotechniczny*, Vol. 90, n. 6, pp. 178-183, 2014.
- [20] European Project EUREMCO, FP7, www.euremco.eu, grant n. 285082.
- [21] J. Bongiorno, A. Mariscotti and N. Pasquino, "Validation of railway electric simulator using scale and slope performance indexes", IMCAS'15, Salerno, 25-29 June, 2015. (Recent Researches in Electrical and Computer Engineering, ISBN 978-1-61804-315-3).